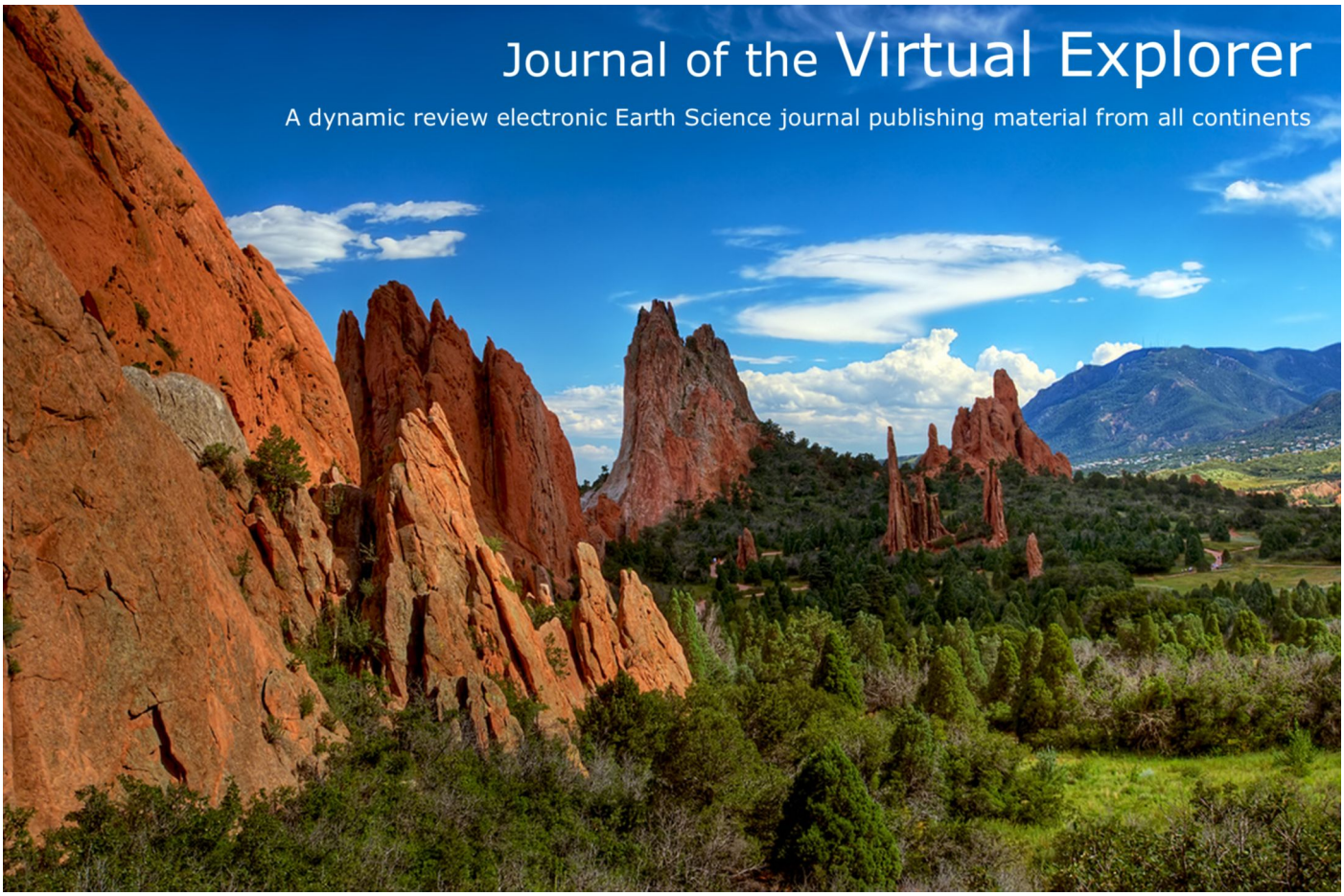

Some important practical issues for the collection and manipulation of Electron Backscatter Diffraction (EBSD) data from geological samples

Angela Halfpenny

Journal of the Virtual Explorer, Electronic Edition, ISSN 1441-8142, volume **35**, paper 3
In: (Eds.) M.A. Forster and John D. Fitz Gerald,
The Science of Microstructure - Part I, 2010.

Journal of the Virtual Explorer, 2010
Volume 35
Paper 3
http://virtualexplorer.com.au/

Some important practical issues for the collection and manipulation of Electron Backscatter Diffraction (EBSD) data from geological samples

Angela Halfpenny

1. Earth Science and Resource Engineering, CSIRO, ARRC, 26 Dick Perry Avenue, Kensington, Western Australia, 6151, Australia. *Email: angela.halfenny@csiro.au*
2. Former address: Research School of Earth Sciences, Australian National University, Canberra, Australia. *Email: angela.halfpenny@anu.edu.au*

Abstract: Due to modern advances in micro-analytical facilities, techniques such as electron backscatter diffraction are becoming the standard tool for performing crystallographic orientation analysis. This has lead to a surge in the numbers of investigations using electron backscatter diffraction analyses. Electron backscatter diffraction allows the systematic measurement of the full crystallographic orientation of grains as small as sub-micron in size in rock-forming minerals as well as other crystalline materials such as metals and ceramics. Performance of electron backscatter diffraction requires samples to be specially prepared and correctly orientated to suit the aims of the research, such as understanding the deformation kinematics of the sample. This paper aims to outline the methodology necessary to go from orientated hand specimen or experimental laboratory sample through to collection of electron backscatter diffraction data. Practical information often omitted from EBSD publications will be presented such as detailed descriptions of sample preparation and discussion about how to achieve good quality results. Guidelines are restricted mainly to the use of Oxford Instruments HKL Channel 5 software and do not cover other analysis hardware and software. However, parts of the paper such as sample preparation and orientation guidelines will be useful to anyone performing EBSD analysis.

Citation: 2010. Some important practical issues for the collection and manipulation of Electron Backscatter Diffraction (EBSD) data from geological samples. In: (Eds.) M.A. Forster and John D. Fitz Gerald, *Journal of the Virtual Explorer*, volume **35**, paper 3, doi: 10.3809/jvirtex.2011.00272

Introduction

In the last decade, micro-analytical facilities have increasingly come to include electron backscatter diffraction (EBSD) (Adams *et al.*, 1993; Dingley, 1984; Venables and Harland, 1973). This application has been rapidly incorporated into the analytical geological toolbox (Prior *et al.*, 1999). EBSD enables the systematic measurement of individual crystallographic orientations that can be used to study microstructures, internal textures, point-to-point orientation correlations, phase identification and distribution, to name but a few examples. EBSD is a scanning electron microscope (SEM) based technique and the necessary equipment can be easily added to most SEM's. The technique can be performed either on a standard SEM with a vertical column and the specimen tilted to achieve the necessary geometry, or on a specialized SEM with an inclined column so the sample remains flat. EBSD is a surface technique, with the signal originating in the top 50nm of the sample (Lloyd, 1987a) and any damage to the crystal lattice in this surface layer will decrease the quality of the electron backscatter pattern (EBSP). Due to advances in computing capabilities and camera technology, data collection speed has increased significantly, allowing larger areas to be studied. From any sample, a single area can be studied using a variety of complementary techniques for instance, element/trace element distributions can be imaged using cathodoluminescence (CL) and measured using energy-dispersive spectroscopy (EDS), wavelength dispersive spectroscopy (WDS) or laser-ablation inductively-coupled-plasma mass-spectrometry (LA-ICP-MS) (Dingley and Randle, 1992; Martin *et al.*, 2010). EBSD data can be used in conjunction with these other techniques to enhance our understanding of the evolution of the sample both structurally and geochemically. It also possible to perform 3D EBSD volumetric mapping by serial sectioning the sample (by repeatedly removing the sample from the SEM and grinding down a small distance) or using focused-ion-beam milling in the SEM to expose new sample surfaces for mapping. EBSD is limited to samples with a crystalline structure and grain sizes larger than several tens of nanometers. This paper presents a systematic methodology for application of EBSD to a sample, discussing how to orientate the sample for analysis, how to prepare the sample surface, guidelines on how to collect high quality EBSD data using Oxford Instruments HKL Channel 5 software and how to manipulate data and present it for interpretation.

Laboratory preparation of samples for EBSD

Orientating samples

Any type of sample can be analysed by EBSD, as long as the sample is crystalline and hard enough to produce a topographically flat surface after polishing. After field mapping has been completed and orientated hand specimens have been collected or laboratory experimental samples have been produced, the most appropriate reference frame to study the sample needs to be chosen (Prior *et al.*, 1987). A common geological reference frame for deformed rocks is the kinematic reference frame where samples are cut perpendicular to foliation and parallel to lineation. This is also referred to as the XZ reference frame (Zucali *et al.*, 2002). For samples produced from laboratory rock deformation experiments it is more applicable to work in a stress-related reference frame, such as using the compression or extension direction as the important external parameter (Llana-Fúnez and Rutter, 2005). A common reference frame for metallurgical research is related to the rolling, normal and transverse directions that correspond to how the metal was processed (Saeid *et al.*, 2010; Siqueira *et al.*, 2011). It is important to record what reference frame is being used as it will be needed during data presentation and interpretation.

It is vital to choose the most applicable reference frame for the research before preparing EBSD samples. It is advisable to keep linear features, whenever possible, parallel to either the long or short axis of the sample (depending upon shape) as this makes data interpretation easier later on. The overall size and shapes of samples that can be studied using EBSD is mainly limited by the size and shape of the SEM EBSD holder. Most holders produced specifically for EBSD analysis (often custom made) will normally accept standard thin sections (30 µm thick slices of rock glued onto glass slides that are often 4.5 x 2.5 cm) and blocks (blocks either rectangular 4.5 x 2.5 cm or 1 inch diameter cylinders). Oversized holders have been made to allow larger samples to be studied and the maximum holder size possible is determined by the size of the SEM sample chamber.

Advanced preparation of samples for EBSD

EBSD can be performed on broken surfaces of samples that do not polish well, but most laboratories work on specially polished sample surfaces. After samples have been cut and polished to produce standard blocks or thin sections, the samples are mechanically polished using decreasing grades of diamond paste such as 3µm, 1µm and either 0.5µm or 0.25µm diamond paste. It is necessary to perform a final stage of polishing to remove the surface layer damaged produced by the previous lapping and mechanical polishing stages. This final damage layer must be removed by an advanced polishing technique such as chemical-mechanical polishing (CMP) (metal and geological specimens), electro-polishing (metals), chemical etching (metals) or ion beam milling (metal and geological specimens). For geological specimens the most common technique used is CMP using either a colloidal silica suspension (0.02-0.06 µm) (Flynn and Powell, 1979; Lloyd, 1987b) or 0.05µm colloidal alumina suspension. This chemical-mechanical polishing process results in very slow abrasion rates removing 1-2 µm of material per hour or ~ 1 atomic monolayer per second (Lloyd, 1987a).

The important differences between the colloidal silica and alumina are the grain shape and pH. Colloidal silica is more rounded in shape and has typical pH values of greater than 9, whereas the alumina suspension has a platy shape and a typical pH value of approximately 7. Different brands of colloidal silica and alumina will have slightly different properties with differences normally being in the grain size and pH. For instance Buehler produces two colloidal silica suspensions which have different pHs and particle sizes, namely (1) MasterMet which is a 0.06µm colloidal silica suspension with a pH of ~10; and (2) MasterMet 2 which is a 0.02µm non-crystallizing colloidal silica suspension with a pH of ~10.5. It is important to make sure to use the suspension which has the properties which suit your task best and which suspension to use depends upon the bulk mineralogy of the thin section and the aims of the research. If part of the aim of the research is to quantify geochemical variations, as well as textural variations, Al is often one of the important constituent elements studied and if the sample is polished with an alumina suspension some of the polishing particles can become embedded into cracks, holes and in the sample surface and may create errors in any geochemical data collected. A good post polishing cleaning routine will reduce this problem but if both silica and alumina suspensions are available and there are no other parameters significantly influencing your choice then colloidal silica is the better option. Due to the pH of colloidal silica many researchers will not use it to polish carbonates as it can cause chemical etching of the sample. Chemical etching can also be a problem if any sample is left to polish for too long a time.

There are many different types of polishing machines and polishing pads available. Polishing pads can be made from cloth that is either stretched out over a disc on the polishing machine or can be attached via an adhesive back. Firms that produce quality equipment and consumables include Buehler, Struers and Kemet. Most of these firms will send out samples so researchers can perform polishing tests on your own equipment to determine the best consumables for your research. Also many of these firms will perform polishing tests on samples supplied to them. When selecting a suitable final stage polishing cloth or pad, choose items that are described as chemically resistant, durable pad ideal for rough and final polishing of hard steels, ceramics and composites for use with CMP or for use with activated suspensions.

Recently I performed a polishing test on a quartz rich sample using a Syntron brand vibratory polishing machine type LP.01C, style B-60693, which operates on 240V, 1.25 amps and 50 cycles. The control dial was turned to 85 (max = 100). A Buehler brand ChemoMet 10” PSA pad and Buehler brand MasterMet colloidal silica were used as the polishing pad and medium. With this setup, the sample needed to be polished for at least 2 hours to produce a surface giving reasonable EBSD patterns. This was slow in comparison to other vibratory polishing machines I have used in the past and the weight of the holder was similar (heavier holder should decrease polishing time). Polishing time of 4-5 hours for this quartz-rich sample gave the best compromise between polishing time and polishing quality. A sample polished for 10 hours showed an extremely high quality polish but this was not absolutely necessary for EBSD. In general, harder materials require more time to polish. Minerals of a similar hardness to quartz should be polished for a similar amount of time.

When performing CMP, the sample requires systematic checking to prevent possible problems such as ‘lifting’ (thin sections) or plucking of grains (thin sections and blocks). ‘Lifting’ in thin sections is a term used to

describe when the rock slice begins to peel away from the glass slide as the polishing fluid flows between the rock slice and glass slide. This can be a common occurrence if using thin sections which were manufactured a long time ago. This is due to the fact that the adhesives used to prepare the thin sections may have degraded over time or were not as high quality as those used in thin section preparation nowadays. If lifting does occur, cease polishing immediately since 'lifted' sample sections cannot be studied using EBSD and the sample will have to be used as is. Plucking of grains causes problems as it reduces the grains available for analysis in the sample but also the loose fragments can scratch the sample surface causing damage to other polished areas.

Post polishing cleaning routines

Figure 1. The effects of polishing and data processing

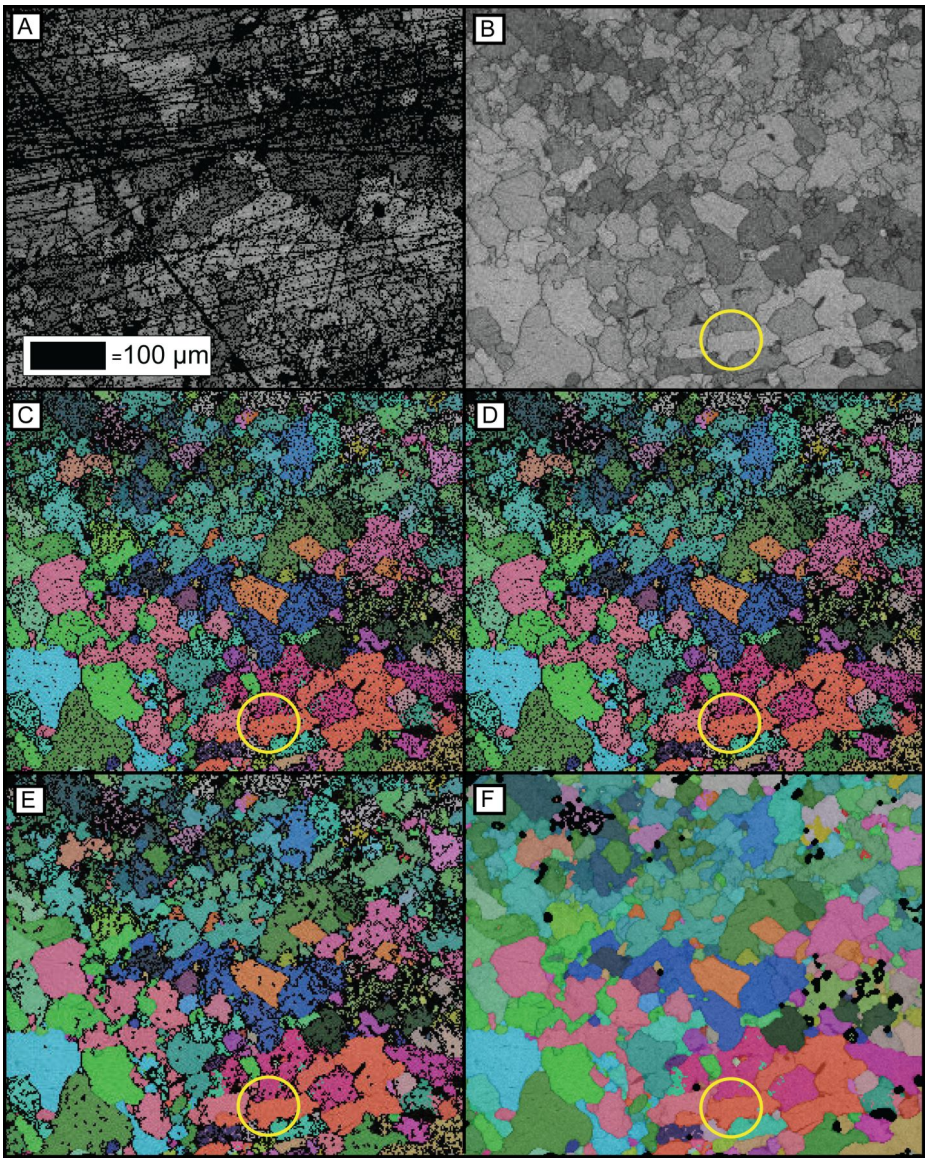

(A) Is an example of a poorly polished sample surface. (B) Is a well polished sample surface where all grains and their boundaries are well defined. This sample is used for remaining figures. (C) The raw EBSD data for an experimentally deformed calcite sample. (D) Illustrates how the 'wildspikes' data processing technique has removed erroneous single data points. Compare the area inside the yellow circle between figures 1C and 1D and the green single pixels have been removed. (E) Displays the data after growth to completion based on 8 and 7 neighbours. (F) Shows the final data after processing is complete.

After the allotted polishing time, check the polished sample using reflected-light on an optical microscope for polishing defects. Figure 1a & 1b illustrate the difference between a poorly polished surface (Fig. 1a) and a well polished surface (Fig. 1b). It is important to thoroughly clean the sample surface to remove all contamination caused during polishing. The sample should be rinsed under cold water, placed into a small beaker of water, and then deposited into an ultrasonic cleaner for approximately ten minutes. This will remove some of the polishing solution particles that have become located in cracks, holes, grain boundaries and embedded into the sample surface. The sample can then be removed from the ultrasonic cleaner and dried using lint free tissues. Another cleaning method is to wipe the surface with ethanol and then allow it to evaporate taking dirt and grease particles with it or dry it using a hot-air dryer. The sample should then be blown off using an inert aerosol spray such as dust off to remove loose particles still attached to the sample surface before being placed into the SEM.

Eliminating charging in the SEM

Electron charging is the buildup of negative charges on a specimen irradiated with an electron beam. Charging may occur in a SEM when there is poor electrical conductivity of the specimen. To eliminate electron charging most mineral samples will need to be coated with a thin conductive film before being placed into the high-vacuum SEM chamber. Depending upon the SEM it is also possible to work under low vacuum and in this case no coating would be required. Also if a sample has a high electrical conductivity then it may not need a conductive coat. When coating is required, carbon is most commonly used as it provides a good electron transparent (low atomic number), conductive coating, but other materials can be used such as gold. Many carbon coaters use a rod of carbon as an evaporation source. Before use, the carbon rods will need to be sharpened to create a tip with the required angle and shape for the coating unit - if this is not done the carbon coat may not be even across the sample. The thickness of the carbon coat needs to be controlled accurately, as a thin coating will cause the sample to charge and a thick coating will reduce the strength of the diffraction patterns and decrease the fraction of successful indexing. While reports vary as to optimal carbon coat thicknesses, such as 2.5-5nm for biominerals (Perez-Huerta and Cusack, 2009) and 8nm for Mg coated standards (Limandri *et al.*, 2010), all of the literature agrees that the carbon coat should be as thin as possible and 3-5nm is generally accepted for EBSD (Bestmann *et al.*, 2011; Trimby and Prior, 1999).

After the conductive coat has been applied to the sample either conductive paint (carbon or silver) or carbon tape is used to make sure any charge build up can be dissipated via the sample holder. The choice of whether to use carbon paint or carbon tape comes down to the geometry of your sample and personal preference. If your sample is a thin section, then you have a slice of rock sitting on top of a glass slide with sharp edges, these edges will only be very thinly coated. In this situation conductive paint is generally the better choice as all edges can be painted to eliminate any possible charging. If your sample is completely flat (thin wafer or sample in resin), then either can be used, although carbon paint is more conductive than carbon tape and silver paint is more conductive than carbon paint.

Scanning electron microscope settings for EBSD

The SEM conditions used to collect your EBSD data depend upon the type of SEM being used, resolution of the camera, phases of interest, desired speed of data collection and desired quality of data. Conventional SEMs utilize thermionic emitters such as tungsten or lanthanum hexaboride (LaB_6) whereas field emission guns (FEG) can use cold-cathode, thermal or Schottky type emittters. The most important difference is that FEGs produce an electron beam which has a smaller diameter and therefore has a higher resolution, which is important if working on fine-grained samples. The specifications of the charge-coupled device (CCD) camera available will affect the quality of the patterns collected and therefore affect the optimum operating conditions. EBSD utilises a geometry with an angle of 70° between the incident beam and the normal to the sample surface. EBSD can be performed at lower angles (such as where the sample stage can only be tilted to 60°) but the quality of the patterns will be reduced. The distance between the phosphor screen (mounted in front of the CCD camera) and the sample is important, the closer the screen is to the beam interaction point, the larger the angular range of the collected EBSP which improves indexing. The downside of this close geometry is the increased risk of collision between the sample and detectors. The spacing between the pole piece and the

sample surface, the working distance, also needs to be matched to the best projection of the EBSP on the phosphor screen. Typical distances are between 14 and 33mm.

Typical accelerating voltages used for EBSD are between 10 and 30kV with most systems using 20kV (Bestmann *et al.*, 2011; Ebner *et al.*, 2010; Okudaira *et al.*, 2010; Peternell *et al.*, 2010; Schwarzer *et al.*, 2009). It is important to note that if the carbon coat is a little too thick a higher accelerating voltage can be used to generate a useable EBSP or if the sample is heavily deformed a lower accelerating voltage may be more appropriate. The beam current is controlled by the chosen aperture size and spot size. A high beam current (10-100nA depending upon the SEM) can be used if mapping very quickly (30-50 points per second in minerals or 300 points per second in metals), but if running more slowly (3-6 points per second) then a lower beam current should be used to avoid unacceptable levels of electron damage. The settings given here are guidelines which will need to be adjusted based upon the hardware and software available as well as the phase(s) to be measured. For an in depth discussion of the factors which affect EBSD patterns see (Britton *et al.*, 2010; Mingard *et al.*, 2011).

Data acquisition settings for EBSD

The settings listed and discussed here are for use with Oxford Instruments HKL Channel 5 program (Schmidt and Olesen, 1989), which currently is the most commonly used software for geological applications. TSL also produces EBSD cameras and their software is called OIM. Bruker and Thermo-Noran also produce their own software and hardware. No two SEMs are exactly the same and these settings are a guide for initiating data acquisition using Oxford Instruments HKL Channel 5 program Flamenco. The specification of the camera being used to collect the data will have a large affect upon the parameters required. These settings can be used for acquiring your first indexed point and should be modified to achieve the best results for the sample being studied, the type of analysis required and the hardware setup. The settings given are from my personal experience and/or from settings published in the literature.

Number of Reflectors: increasing the number of reflectors is necessary in lower symmetry crystals to allow accurate determination of the orientation. The higher the symmetry the fewer reflectors are needed.

Number of Bands: the Channel 5 software allows the minimum and maximum number of bands to be defined, but these can be the same number.

Band Centers verses Band Edges: if the EBSP exhibits well defined band edges in the collected pattern, then band edges should be used, as this provides extra information later, but if the centre of the band is clear and the band edges are fuzzy, then band centers should be used instead.

Hough Resolution: the higher the Hough resolution, the more likely it is to be correctly indexed, but increasing the Hough resolution will increase the time per point required to index the pattern. So the value used is a trade-off between the percentage of correctly indexed data points and the time required to collect the data. For in depth discussions of the Hough transform see Dingley and Randle, (1992) and Hough, (1962).

Number of frames noise reduction: increasing the number of frames averaged to generate each EBSP improves the signal-to-noise ratio and causes an increase in the percentage of correctly indexed grains but increases the collection time at each point.

Each time you analyse a sample you will need to optimize the data acquisition settings and the calibration for that run to ensure you achieve the maximum amount of indexing possible at the fastest analysis rate. It is important to note that when indexing only one phase the parameters can be set which result in the fastest indexing rate to correctly indexed data points. When multiple phases are being analysed, the set of conditions used has to be a compromise between those for the individual phases.

Table 1. Suggested initial parameter settings for data acquisition using HKL Channel 5's Flamenco program

Phase	No. of Reflectors	Minimum no. of Bands	Maximum no. of Bands	Hough resolution	No. of frames noise reduction	Reference
Quartz	70-75	7-8	7-8	90-120	2-3	(Bestmann *et al.*, 2011; Halfpenny *et al.*, 2006)
Calcite	60-100	7-9	7-9	60-100	1-3	(Bestmann *et al.*, 2006)
Feldspar	60-75	4-6	6-8	60-120	3-4	(McLaren and Reddy, 2008)
Hornblende	70-75	6-7	7-8	90-120	2-4	Personal experience
Clinopyroxene	70-75	6	8	120	3	(Bascou *et al.*, 2001)
Orthopyroxene	70-80	6-7	8-9	90-120	3-4	Personal experience
Garnet	50-80	4-6	6-8	90-120	3	(Bestmann *et al.*, 2008)
Olivine	75	6-7	7-8	120	3	(Bystricky *et al.*, 2006)
Pyrite	60-120	6-7	8-9	100	3	(Barrie *et al.*, 2008)
Magnetite	60-75	4-7	5-8	80	3	(Morales *et al.*, 2008)
Ilmenite	75-80	6-7	7-8	70-80	2-3	Personal experience
Zircon	75	6	10	60	4	(Reddy *et al.*, 2007)

Data collection methodology

The way EBSD data is collected will vary depending upon the type of analysis desired. There are three methods for data collection (1) collecting individual points (2) collecting a line of points (3) collecting an XY controlled systematic grid of points usually known as a map (single or multiple maps can be collected). EBSD data collection can be integrated with chemical analysis by simultaneously collecting EDS at each analysis point. Performing integrated analysis increases the time required to collect the data at each point but has the advantages of having co-located structural and geochemical data.

Point analysis is most commonly used to determine the orientation of a single crystal, to confirm that the crystal is a single orientation (take multiple points in one crystal and check the orientation does not change), to verify or identify phases or to compare the orientation of multiple crystals (collect a single point in each crystal and compare the orientations). When point analyses are being performed the researcher controls the location of the beam, choosing the sites to be analysed manually. Once the EBSP is generated the software will provide indexing solution(s) which the researcher goes through manually to choose the correct solution, which will then be saved. With this manual data collection method no non-indexed or mis-indexed points will be saved. This data can be presented using either pole figures or orientation distribution functions (ODF).

Line scans collect a line of systematically spaced data points and are usually performed to analyse grain sizes, it is the same principle as the linear intercept method (Thorvaldsen, 1997). The advantages of performing line scans using EBSD, rather than on an optical microscope are that smaller grains can be identified, it is more accurate and you also get orientation information on the grains analysed which may reveal information about internal substructure. Again this data can be presented using either pole figures or ODFs.

Maps are required to answer more complicated questions about issues such as rheology or controlling deformation mechanisms or active slip systems. Maps provide the most information but also take the longest time to collect. Map data can be collected in two ways, either by using low magnification and collecting one large map, or by using higher magnification and collecting multiple smaller maps. The multiple maps can be combined into one map using software called *Map Stitcher*. The

downside of multi-mapping is that occasionally the stitched maps do not fit together exactly and low angle boundaries are artificially produced at the overlapping locations. Multi-mapping tends to be used when a large area needs to be covered at a magnification that does not allow the entire area of interest to fit on one screen. This is common when you have bi-modal grain sizes associated with, for example, recrystallised or porphyritic textures.

As maps are collected automatically the data will inevitably contain non-indexed points (points with no orientation solution generated at grain boundaries, cracks and surface particles) and mis-indexed points (points with an incorrect solution, either the wrong orientation or the wrong phase). Therefore maps will require data processing to decrease/remove any non-indexed points and mis-indexed points. This has to be done carefully so that no artifacts (incorrect data) are produced (this is discussed later in Data Processing). The data acquisition settings for EBSD should be optimized to produce as few non-indexed and mis-indexed points as possible. The percentage of indexed analysis points required for the raw (uncorrected) data to be useable depends on the type of sample being analysed and what the aims of the research are. If the sample is made up of phenocrysts contained within a non-crystalline groundmass and maps are performed to capture multiple phenocrysts, the indexing could be as low as 5-10% but the data is useable as the phenocrysts are completely indexed and all the non-indexed points are located in the groundmass. In a sample which contains several phases or just multiple grains, 100% indexing cannot be achieved due to the grain boundaries. In these situations maps with raw indexed rates of less than 50% (more incorrect solutions than correct solutions) should be used with caution. XY grid collected data can be presented as maps, pole figures or ODFs.

Both line scan and map data collection can be automated by defining the start and end location (in the *Flamenco* software) but there are two data collection methods used in automated EBSD, stage scan or beam scan. In stage-scan mode the stage mechanically steps between each data point and the incident beam remains stationary (Adams *et al.*, 1993), whereas in beam-scan mode the incident beam is deflected across the sample surface while the stage remains stationary. Currently it is much faster to deflect the beam rather than move the stage when performing line scans or maps. If multiple maps are being collected then the beam will be scanned across the defined area of a single map then the stage will move to the XY starting coordinates of the next map and the mapping process will resume until all maps have been collected. It is also possible to save all of the generated EBSPs so the patterns can be reanalysed offline by hand to check for and correct mis-indexed and non-indexed points. This can be extremely important when analysing challenging materials.

Data processing

If the data have been collected automatically as maps, the data will need to be corrected for non-indexed and mis-indexed points and is essential to eliminate errors and artifacts. The amount of data processing required will depend upon how well the raw data indexed and what the data will be used for (Bestmann and Prior, 2003; Prior *et al.*, 2002; Toy *et al.*, 2008). Once the raw EBSD data has been collected (Fig. 1c) a good way to start is to remove the ‘wildspikes’, single data pixels that are surrounded by 8 pixels of a different orientation. When the software removes each ‘wildspike’ it assigns the pixel an average orientation of the surrounding 8 neighbours (Fig. 1d). This is only appropriate in raw data sets with high indexing rates and low mis-indexing rates (Prior *et al.*, 2009). The justification for doing this first is that the next step of data processing involves ‘growth’ and growing incorrect data points could introduce artifacts into the data.

It is common in geological raw data sets for indexing and mis-indexing rates to be heterogeneous whereby one grain is fully indexed and contains no errors yet the adjacent grain is only, say, 80% indexed and contains mis-indexed points. In these cases it is necessary to ‘grow’ the grains using the extrapolation routines in HKL’s *Tango* program. The *Tango* software allows non-indexed points to be filled with the average orientation of a specified number of neighbour pixels (where their orientation is the same within a defined tolerance). The software allows the number of neighbours to be altered to allow more or less growth to take place. Growth to completion on the basis of 8, 7, 6, neighbours does not create significant microstructural artifacts, nor does a single step at 5 neighbours (Prior *et al.*, 2009). Figure 1e shows how the data looks after the wildspikes have been removed and growth to completion at 8 and 7 neighbours, whereas figure 1f shows the data after growth to completion at 6 and 5 neighbours plus one step at 4. Comparison of figure 1b

and 1f shows that the boundary structure is still equivalent and no artifacts have been introduced. If you compare the grain that is inside the yellow circle between each of the maps, it shows how the 'wildspikes' (green coloured pixels) are apparent in figure 1c but removed by figure 1d and that non-indexed points (black pixels) are completely removed after the data processing is complete (Fig. 1f). After this type of data processing has been completed, continued growth based on fewer neighbours can introduce significant errors into the data set. Introduced errors can be identified and avoided by continuously comparing the processed data with the pattern quality map (which for the purpose can be assessed like a backscattered electron image). As soon as grains 'grow' so that the new positions of their grain boundaries cross those of the pattern-quality component map, then artifacts have been introduced and the data processing has gone too far. For more complicated ways to perform data processing see Prior *et al.*, (2009).

Data presentation

The HKL software allows multiple data presentation methods such as maps (*Tango*), pole figures (*Mambo*), inverse pole figures (*Mambo*) and ODFs (*Salsa*). Each method is used to interrogate a specific aspect of the data. The data shown in Figures 1b-f, 2, 3, 4 and 5 are for an experimentally deformed calcite sample.

Maps

Maps can only be plotted from data collected in the XY grid mapping mode. Point data and line scans cannot be plotted up as maps. Maps are used to illustrate the overall microstructure and allow different aspect of the maps to be interrogated such as grain size variations, low angle grain boundaries, high angle grain boundaries, the type and location of twins, phase distribution, inter-phase relationships and much more. A few examples are shown in figure 2. The maps are created by using single or multiple components. Each component is designed to highlight a particular aspect of the microstructure such as the misorientation angle of the boundaries or the distribution of phases. Multiple components can be used on one map and these types of overlain maps are used to understand the inter- and intra-grain relationships.

Figure 2a shows the band-contrast or pattern-quality component overlain by the boundary component, where each colour represents a defined range of misorientation angles: ≥2° = yellow, ≥5° = green, ≥10° = blue, ≥20° = pink and ≥30° = black. In the band-contrast map the grayscale of each pixel reflects the definition of the pattern regardless of index result, where darker shades are of poorer pattern quality and generally correspond to grain/phase boundaries. The signal can be affected by the diffraction intensity for the phase, the dislocation/crystallographic defect density and the orientation. The boundary component draws boundaries between map pixels where the orientation change is greater than the user defined minimum. Depending upon the phase boundaries with misorientation angles of less than 10° (different angles can be selected for different phases), are defined as low-angle grain boundaries, whereas boundaries with misorientation angles of greater than 10° are classed as high-angle grain boundaries. The boundary component shows the distribution and concentration of boundaries but it is also possible to show the percentage of boundaries which display particular misorientation angles using the misorientation angle distribution bar chart.

Special boundaries can be plotted using specific axis-angle relationships corresponding to known twin laws (Halfpenny, 2011), or phase boundaries. It is also possible to map complicated phase boundaries such as specific exsolution texture relationships. Special boundaries can also be used to determine previously unknown axis-angle relationships either between grains or intra-grain. In figure 2a inside the yellow circle is a light blue coloured boundary which represents an E-twin. The sample contains surprisingly few E-twins for a deformed calcite sample. The ability to highlight special boundaries is an important feature as the type of twinning can be used to understand the deformation mechanisms and evolution of a sample and the locations of phase boundaries can illustrate angular relationships between layers.

Figure 2. Example maps produced using HKL Channel 5 Tango software

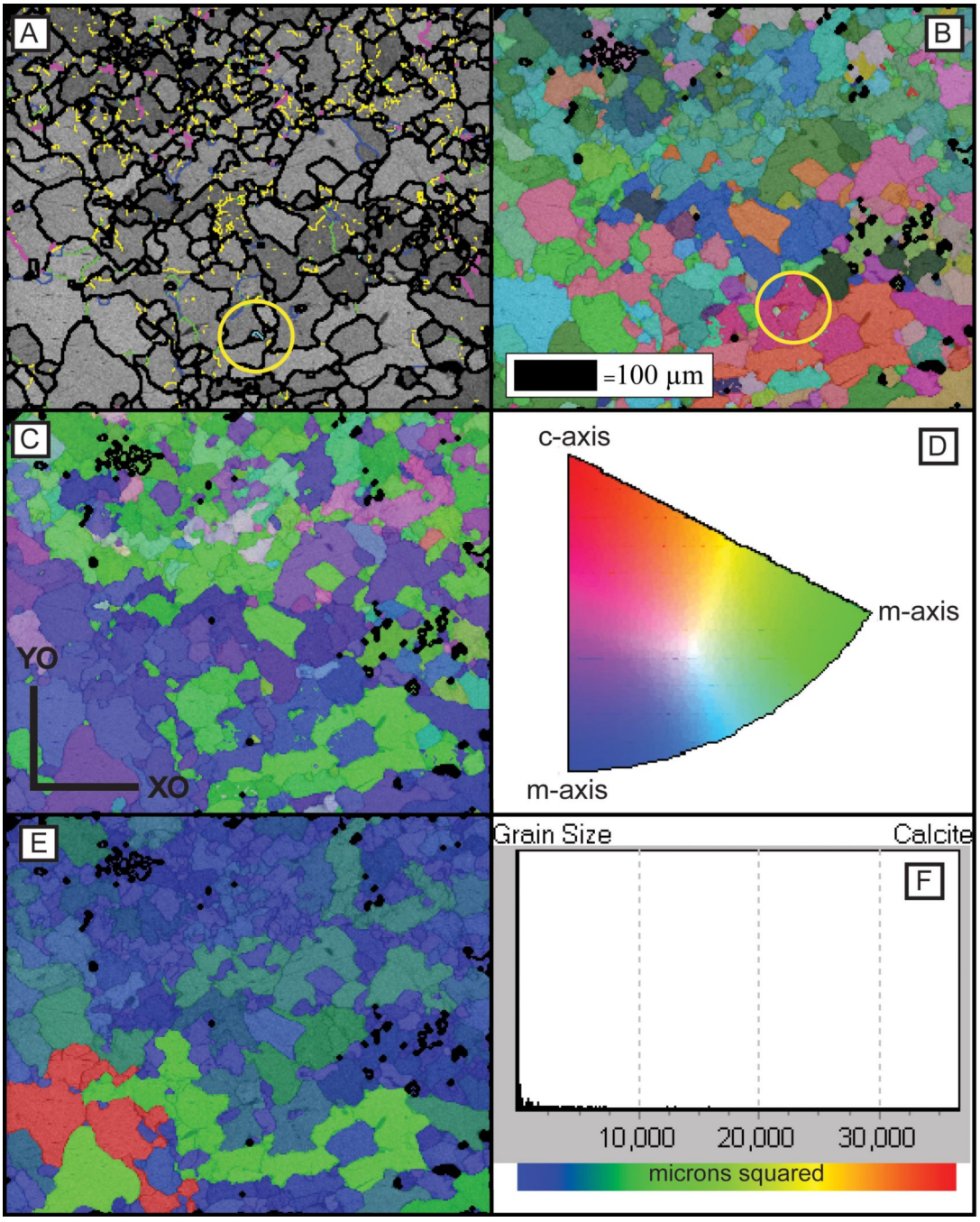

(A) Shows the band-contrast or pattern-quality component overlain by a boundary component, where each colour represents greater than or equal to a defined misorientation angle: ≥2° = yellow, ≥5° = green, ≥10° = blue, ≥20° = pink, and ≥30° = black and also the e-twin special boundary component which colours e-twins in light blue. An e-twin example is highlighted inside the yellow box. (B) Grains coloured according to their crystallographic orientation expressed using Euler angles, φ1, Φ, φ2 semi-transparently overlain on the band-contrast component. (C) Grains coloured with the inverse pole figure component shown in figure 2D. (D) IPF crystal reference frame of colours used to produce the map shown in figure 2C. (E) Grains coloured with a grain size (area µm^2) component from red (large) to blue (small) (see figure 2F) semi-transparently overlain on the band-contrast component. (F) Shows the legend for the colour scheme used in figure 2E.

Figure 2b plots grains coloured according to their measured crystallographic orientation expressed using Euler angles, φ1, Φ, φ2 (Dingley and Randle, 1992), in general similar colours indicate similar orientations and

these maps are used as a display the texture of the overall microstructure. Euler maps clearly show preferred orientations and layering. Euler colouring is used in *Tango* to assign each Euler angle to a red, green, and blue colour and the three are combined into a single RGB colour per pixel. A full definition of Euler angles and Euler space can be found in (Wenk, 1985). In figure 1f inside the yellow circle is a deep pink grain that contains some green areas. These areas are not mis-indexed points which require removal via data processing but are actually within a couple of degrees of the rest of the grain. This "wraparound" effect is due to how the colours are assigned based on the measured Euler angles. This happens when one or more of the Euler angles are near a limit, causing the R, G, or B component to vary between maximum and minium, giving vast colour differences where little or no orientation change occurs. Due to this limitation it may be more applicable to use another colouring scheme such as inverse pole figure (IPF) colouring. It is important to note that all orientation colouring schemes have some sort of limitation.

In figure 2c, the grains are coloured according to the IPF component semi-transparently overlain on the band contrast component (for background on IPF's, see Law *et al.* (1986)). The IPF colour scheme is shown in figure 2d. The inverse pole figure component uses a basic RGB colouring scheme, to fit the IPF appropriate for the crystallography of the phase. For trigonal, red, green and blue are assigned to grains whose c-axis or m-axes, respectively, are parallel to the user-defined projection direction of the IPF. In this case the map is dominated by blue and green coloured grains which have m-axes parallel to XO (the user-defined projection direction). IPF component colouring is most useful for understanding preferred orientations and viewing internal substructure. This component works on all crystal systems except for triclinic. IPF colouring is not susceptible to the "wraparound" effect but does have a limitation - two crystals which share the crystallographic axes that is parallel to the specified IPF projection direction but can possess significantly different orientations are coloured the same.

Grain size is an important parameter in understanding the nucleation and recrystallisation mechanisms a sample has been subjected to. Grain size distribution can be revealed readily via maps. Figure 2e is coloured based upon the grain size component utilizing a rainbow colour scheme from red (largest) to blue (smallest) semi-transparently overlain on the band contrast component. The legend for the colour scheme is shown in figure 2f. The map shows very few original large grains because deformation has reduced the grain size. These maps are extremely useful when analysing bi-modal grain size samples such as highly deformed samples where protolith grains will be large and recrystallised grains will be small.

Map data is extremely powerful as it allows the microstructure to be separated into subsets, so specific features can be studied. An example would be separating the data into recrystallised grains and protolith grains. In this way, grain size calculations can be performed individually for each subset and the texture of each subset can be plotted to provide information about the controlling recrystallisation and nucleation mechanism. Other common applications of subset creation involve polyphase samples where individual texture and orientation relationships can be divided into individual phases to interrogate the P-T-t path. Subsets are an extremely powerful way of interrogating the data, especially in complicated samples. Maps can also be used to study aspects of single grains, for example internal misorientation distribution. This can be used to determine the controlling slip-system(s).

Pole figures

Pole figures can be plotted no matter how the data have been collected and are most commonly used for texture analysis, for confirming single crystal orientation and for studying slip systems. It is important to present data in the most suitable reference frame for the research. If the XZ kinematic reference frame is selected, then Z conventionally plots at the north position and X plots at the east position. In figure 3, the sample was deformed under extension and the data is presented with the extension direction plotting along the vertical axis and is represented by a pair of opposed arrows (Fig. 3). Figure 3a plots every measured data point from the map as point data (poles to the planes). Figure 3b shows the same data but contoured. Sometimes it is not necessary to contour the data as the texture can clearly be seen from the point data (as in this case) but at times there are so many data points that the plot is covered and no relationship can be clearly defined from the point data alone.

Figure 3. Pole figures produced using HKL Channel 5 Mambo software

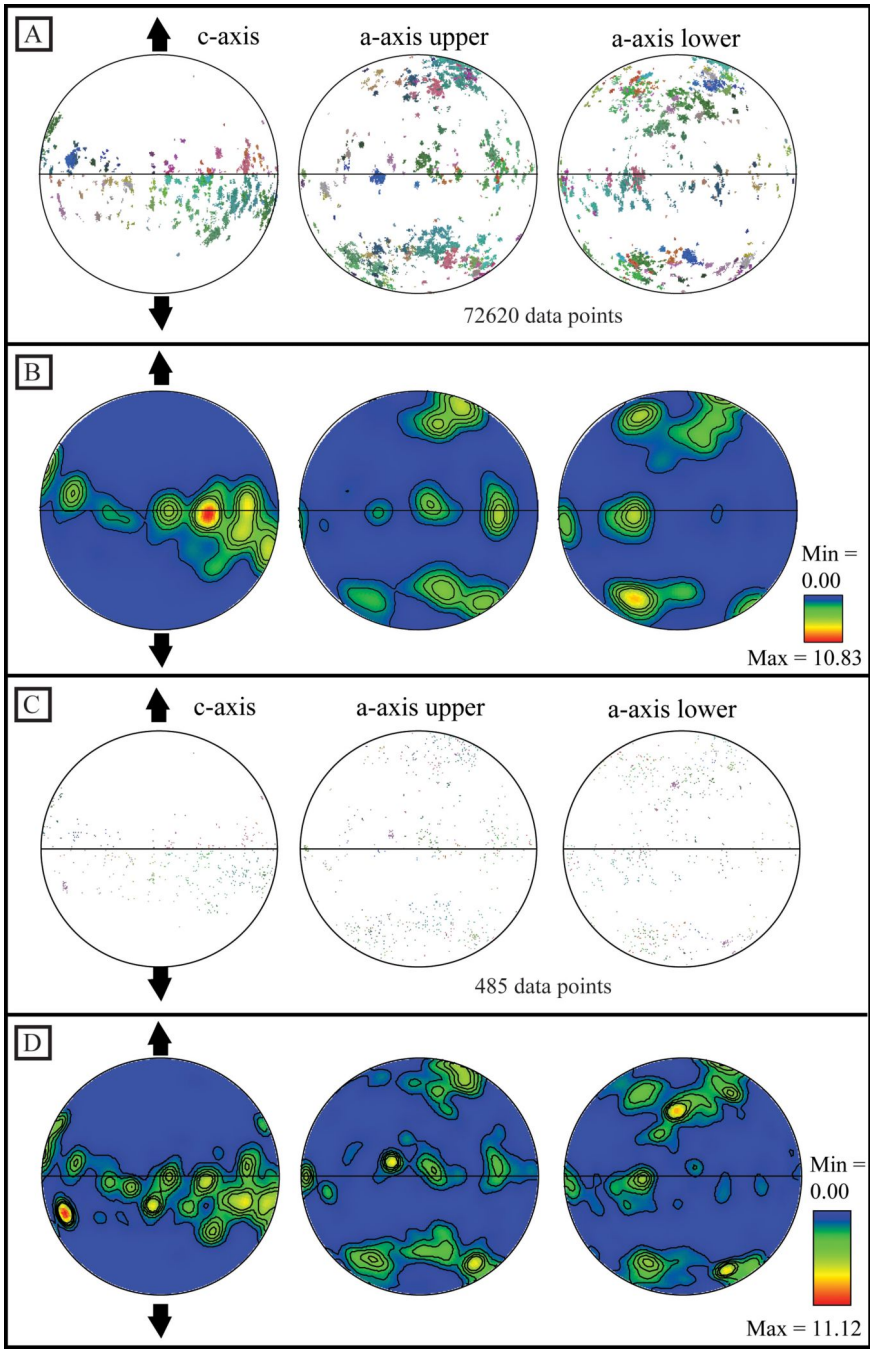

Equal area, lower hemisphere pole figures, with the experimental extension direction marked plotting: (A) Point data plot for all data points (72620), the colours correspond to figure 2b. (B) Contour plot of the same data shown in figure 3A, where the half width used is 15° and the data clustering was 5°. (C) One point per grain data for the same area (495 data points), the colours correspond to figure 2B. (D) Contour plot of the same data shown in figure 3C, where the half width used is 15° and the data clustering was 5°.

Data must be contoured to quantify the texture strength. Figure 3b exhibits a maximum texture strength of 10.83 times random, which is significant. There are other methods for comparing texture strength such as Kearns factors (Gruber *et al.*, 2011), the J-index (Mainprice and Silver, 1993) and the M-index (Skemer *et al.*, 2005), Kearns factors can be calculated in *Mambo* but to calculate J- and M- index the data has to be exported into another program such as excel. How the data is contoured is also important as it will sharpen or weaken

the appearance of the contoured data but more importantly it will change the calculated texture strength. So when performing a comparison it is important to always use the same contouring conditions. Figure 3b was produced with a half width of 15° and data clustering set to 5° and plotted on equal-area, lower-hemisphere pole figures. The data in figure 3 show a-axes split into upper and lower hemispheres as required by the trigonal crystal symmetry.

The data in figure 3a and 3b were produced using every measured data point but each grain will contain multiple data points and these will cause a cluster on a pole figure. If the aim of the research is to compare texture with volume then this methodology is appropriate but single point-per-grain can be used for the analysis, to ensure the CPO is real and not an artifact of over sampling of the large grains. Figures 3c and 3d plot only one point per grain for the same areas as shown in figures 3a and 3b. The number of data points used has been significantly reduced from 72620 to 495, the number of grains contained within the mapped area. Texture strength when using all of the data points is 10.83 compared to the one point per grain value of 11.12. Also if you compare the contoured pole figure plots (Fig. 3b and 3c), 3c is a better representation of the point data and is therefore more realistic and a better display of the CPO. These are the most common methods used for creating contoured pole figure data but there are others (Halfpenny *et al.*, 2006).

Inverse pole figures

Figure 4. Misorientation data plotted using inverse pole figures

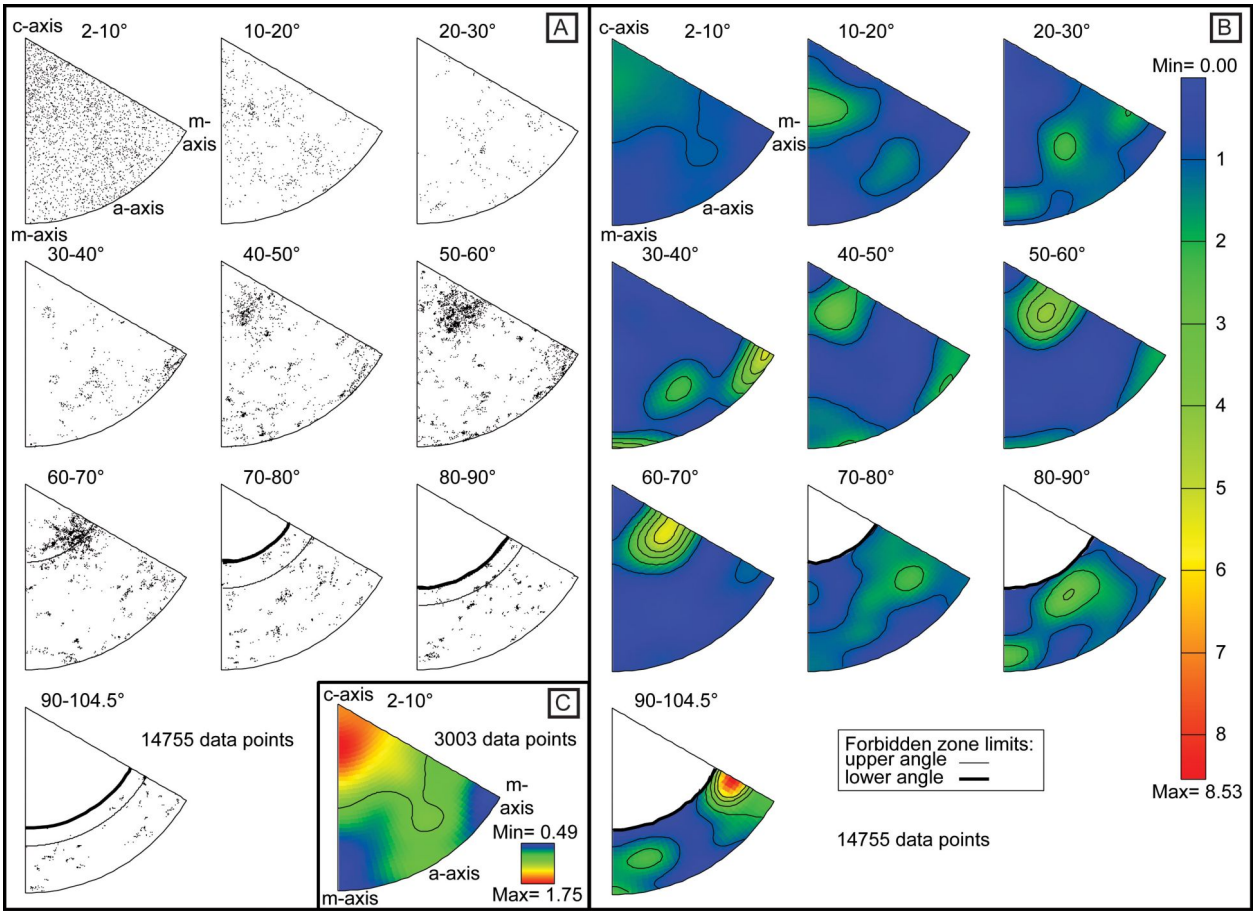

Misorientation angle/axis pair data plotted up in 10° intervals of misorientation on inverse pole figures. (A) Raw point data. (B) Contour plot of the same data shown in figure 4A, where the half width used is 15° and the data clustering was 5°. (C) Separates off the 2-10° plot and contours it singularly (contoured using the same settings as figure 4B).

Inverse pole figures can be used in place of traditional pole figures (plotting the same data as on the pole figure or highlighting fiber textures discussed in the IPF map component section) or for misorientation analysis (plotting the misorientation angle/axis data pair data relationships). For discussions on how IPF's are generated please see (Law *et al.*, 1986; Lloyd and Ferguson, 1986; Lloyd *et al.*, 1987; Lloyd and Law, 1987; Randle, 1995). The data shown in figure 4 are misorientation angle/axis pair relationships. These data illustrate which axes dominate the rotation geometry and allow the determination of controlling slip systems or twin laws. Also the data can be used to indicate mechanisms that have caused microstructural modification such as grain boundary sliding.

Figure 4a shows the point data separated out into 10° slices up to the maximum allowed rotation (104.5°) due to the trigonal crystal class. Figure 4b shows the same data as in 4a but contoured using a half width of 15° and a cluster size of 5. Figure 4c is contoured using the same conditions as in figure 4b and is shown to illustrate the fact that when multiple plots are contoured at the same time, all of the plots are contoured relative to each other. If each plot is contoured individually there is no loss of data (compare figure 4c with the first plot 2-10° in 4b) and the variations can be seen more clearly. The white zones on the plots for misorientation angles > 70° are symmetry related since no rotations can exist in these zones. The data show that for internal subgrain boundaries (plot 2-10°) the rotations are around the c-axis with some rotations about the a-axes whereas at higher angles the dominant rotation axes are e and m.

Orientation distribution functions

ODF's are used to illustrate texture. ODF's are not commonly used in the geological sciences but are the standard viewing method for orientation analysis in materials science. There is some literature applying ODFs to geological samples: (Bunge, 1981; Bunge *et al.*, 1989; Law, 1987; Law *et al.*, 1990; Mainprice *et al.*, 1993; Russell and Ghomshei, 1997; Schmid *et al.*, 1981) but it is difficult to use ODFs to illustrate twin relationships. ODFs are more suited for studying samples where the relationship between the anisotropic properties of single crystals and the polycrystalline material are being compared (Bunge, 1981).

Summary

- EBSD provides quantified analysis of crystallographic data that can either be handpicked from important locations or systematically collected along lines or XY grids.
- It is important to define the focus of the research before samples are even cut as the plane of sectioning will have important controls upon the information which can be gathered.
- Most crystalline minerals can be measured using EBSD. Phyllosilicates (including clays and micas) remain problematic.
- A very high standard of sample finish is essential for the collection of high quality data and is not an insignificant task but is not unmanageable either.
- Meticulous data processing is crucial for geological applications.
- The benefits of EBSD are in the versatility of the data that can be used for a wide range of investigations such as using CPOs to calculate the anisotropic properties of minerals and rocks, to constrain dislocation slip systems, to understand recovery and recrystallisation mechanisms, or to determine twin laws. These represent just a few of the possible examples.

Acknowledgements

I would like to thank Anna Hutchens taking time out from her busy schedule to help with the motivation and editing of this paper. I would also like to thank Ian Jackson and John Fitzgerald for their constructive comments. I would like to thank the two reviewers Auke Barnhorn and Patrick Trimby for their constructive comments which improved the manuscript. Data collected at the University of Liverpool funded by a NERC research studentship tied to Grant Number NER/A/S/2001/01181. Sample deformed at the University of Manchester by Walliad Ismail.

References

Adams, B.L., Wright, S.I., Kunze, K., 1993. Orientation Imaging - the Emergence of a New Microscopy. Metallurgical Transactions a-Physical Metallurgy and Materials Science 24, 819-831.

Barrie, C.D., Boyle, A.P., Cox, S.F., Prior, D.J., 2008. Slip systems and critical resolved shear stress in pyrite: an electron backscatter diffraction (EBSD) investigation. Mineralogical Magazine 72, 1181-1199. 10.1180/minmag.2008.072.6.1181

Bascou, J., Barruol, G., Vauchez, A., Mainprice, D., Egydio-Silva, M., 2001. EBSD-measured lattice-preferred orientations and seismic properties of eclogites. Tectonophysics 342, 61-80. 10.1016/S0040-1951(01)00156-1

Bestmann, M., Habler, G., Heidelbach, F., Thöni, M., 2008. Dynamic recrystallization of garnet and related diffusion processes. Journal of Structural Geology 30, 777-790. 10.1016/j.jsg.2008.02.007

Bestmann, M., Pennacchioni, G., Frank, G., Göken, M., de Wall, H., 2011. Pseudotachylyte in muscovite-bearing quartzite: Coseismic friction-induced melting and plastic deformation of quartz. Journal of Structural Geology 33, 169-186. 10.1016/j.jsg.2010.10.009

Bestmann, M., Prior, D.J., 2003. Intragranular dynamic recrystallization in naturally deformed calcite marble: diffusion accommodated grain boundary sliding as a result of subgrain rotation recrystallization. Journal of Structural Geology 25, 1597-1613.10.1016/S0191-8141(03)00006-3

Bestmann, M., Prior, D.J., Grasemann, B., 2006. Characterisation of deformation and flow mechanics around porphyroclasts in a calcite marble ultramylonite by means of EBSD analysis. Tectonophysics 413, 185-200. 10.1016/j.tecto.2005.10.044

Britton, T.B., Maurice, C., Fortunier, R., Driver, J.H., Day, A.P., Meaden, G., Dingley, D.J., Mingard, K., Wilkinson, A.J., 2010. Factors affecting the accuracy of high resolution electron backscatter diffraction when using simulated patterns. Ultramicroscopy 110, 1443-1453. 10.1016/j.ultramic.2010.08.001

Bystricky, M., Heidelbach, F., Mackwell, S., 2006. Large-strain deformation and strain partitioning in polyphase rocks: Dislocation creep of olivine-magnesiowüstite aggregates. Tectonophysics 427, 115-132. 10.1016/j.tecto.2006.05.025

Dingley, D.J., 1984. Diffraction from Sub-Micron Areas Using Electron Backscattering in a Scanning Electron-Microscope. Scanning Electron Microscopy, 569-575.

Dingley, D.J., Randle, V., 1992. Microtexture Determination by Electron Back-Scatter Diffraction. J. Mater. Sci. 27, 4545-4566. 10.1007/BF01165988

Ebner, M., Piazolo, S., Renard, F., Koehn, D., 2010. Stylolite interfaces and surrounding matrix material: Nature and role of heterogeneities in roughness and microstructural development. Journal of Structural Geology 32, 1070-1084. 10.1016/j.jsg.2010.06.014

Flynn, G.W., Powell, W.J.A., 1979. The Cutting and Polishing of Electro-Optic Materials. Wiley, New York.

Gruber, J.A., Brown, S.A., Lucadamo, G.A., 2011. Generalized Kearns texture factors and orientation texture measurement. J. Nucl. Mater. 408, 176-182. 10.1016/j.jnucmat.2010.11.031

Halfpenny, A., 2011. Application of EBSD to Oceanic Gabbros: Insights into an Oceanic Core complex, Australian Microscopy & Microanalysis Newsletter, pp. 42-44.

Halfpenny, A., Prior D.J., Wheeler, J., 2006. Analysis of dynamic recrystallization and nucleation in a quartzite mylonite. Tectonophysics 427, 3-14. 10.1016/j.tecto.2006.05.016

Hough, P.V.C., 1962. Method and Means for Recognizing Complex Patterns. -U.S. Patent, 3069654.

Law, R.D., Casey, M., Knipe, R.J., 1986. Kinematic and tectonic significance of microstructures and crystallographic fabrics within quartz mylonites from the Assynt and Eriboll regions of the Moine thrust zone, NW Scotland. Transactions of the Royal Society of Edinburgh 77, 99-126.

Limandri, S.P., Carreras, A.C., Trincavelli, J.C., 2010. Effects of the carbon coating and the surface oxide layer in electron probe microanalysis. Microsc Microanal 16, 583-593. 10.1017/S1431927610093761

Llana-Fúnez, S., Rutter, E.H., 2005. Distribution of non-plane strain in experimental compression of short cylinders of Solnhofen limestone. Journal of Structural Geology 27, 1205-1216. 10.1016/j.jsg.2004.08.013

Lloyd, G.E., 1987a. Atomic-Number and Crystallographic Contrast Images with the Sem - a Review of Backscattered Electron Techniques. Mineralogical Magazine 51, 3-19. 10.1180/minmag.1987.051.359.02

Lloyd, G.E., 1987b. Fabric Analysis Using Sem Electron Channeling. J. Geol. Soc. 144, 678-678.

Lloyd, G.E., Ferguson, C.C., 1986. A Spherical Electron-Channeling Pattern Map for Use in Quartz Petrofabric Analysis. Journal of Structural Geology 8, 517-526. 10.1016/0191-8141(86)90002-7

Lloyd, G.E., Ferguson, C.C., Law, R.D., 1987. Discriminatory Petrofabric Analysis of Quartz Rocks Using Sem Electron Channeling. Tectonophysics 135, 243-249. 10.1016/0040-1951(87)90165-X

Lloyd, G.E., Law, R.D., 1987. A spherical electron channelling pattern for use in quartz petrofabric analysis: correction and varification. Journal of Structural Geology 9, 251-253. 10.1016/0191-8141(87)90031-9

Mainprice, D., Silver, P.G., 1993. Interpretation of SKS-waves using samples from the subcontinental lithosphere. Physics of the Earth and Planetary Interiors 78, 257-280. 10.1016/0031-9201(93)90160-B

Martin, L. A. J., M. Ballevre, et al. (2011). "Garnet re-equilibration by coupled dissolution-reprecipitation: evidence from textural, major element and oxygen isotope zoning of 'cloudy' garnet." Journal of metamorphic geology 29(2): 213-231. 10.1111/j.1525-1314.2010.00912.x

McLaren, S., Reddy, S.M., 2008. Automated mapping of K-feldspar by electron backscatter diffraction and application to 40Ar/39Ar dating. Journal of Structural Geology 30, 1229-1241. 10.1016/j.jsg.2008.05.008

Mingard, K., Day, A., Maurice, C., Quested, P., 2011. Towards high accuracy calibration of electron backscatter diffraction systems. Ultramicroscopy 111, 320-329. 10.1016/j.ultramic.2011.01.012

Morales, L.F.G., Lagoeiro, L.E., Endo, I., 2008. First results on the LPO-derived seismic properties of iron ores from the Quadrilátero Ferrífero region, southeastern Brazil. Tectonophysics 460, 21-33. 10.1016/j.tecto.2008.06.021

Okudaira, T., Ogawa, D., Michibayashi, K., 2010. Grain-size-sensitive deformation of upper greenschist- to lower amphibolite-facies metacherts from a low-P/high-T metamorphic belt. Tectonophysics 492, 141-149. 10.1016/j.tecto.2010.06.002

Perez-Huerta, A., Cusack, M., 2009. Optimizing Electron Backscatter Diffraction of Carbonate Biominerals-Resin Type and Carbon Coating. Microscopy and Microanalysis 15, 197-203. 10.1017/S1431927609090370

Peternell, M., Hasalová, P., Wilson, C.J.L., Piazolo, S., Schulmann, K., 2010. Evaluating quartz crystallographic preferred orientations and the role of deformation partitioning using EBSD and fabric analyser techniques. Journal of Structural Geology 32, 803-817. 10.1016/j.jsg.2010.05.007

Prior, D.J., Boyle, A.P., Brenker, F., Cheadle, M.C., Day, A., Lopez, G., Peruzzo, L., Potts, G.J., Reddy, S., Spiess, R., Timms, N.E., Trimby, P., Wheeler, J., Zetterstrom, L., 1999. The application of electron backscatter diffraction and orientation contrast imaging in the SEM to textural problems in rocks. American Mineralogist 84, 1741-1759.

Prior, D.J., Knipe, R.J., Bates, M.P., Grant, N.T., Law, R.D., Lloyd, G.E., Welbon, A., Agar, S.M., Brodie, K.H., Maddock, R.H., Rutter, E.H., White, S.H., Bell, T.H., Ferguson, C.C., Wheeler, J., 1987. Orientation of Specimens - Essential Data for All Fields of Geology. Geology 15, 829-831. 10.1130/0091-7613(1987)15<829:OOSEDF2.0.CO;2

Prior, D.J., Mariani, E., Wheeler, J., 2009. EBSD in the Earth sciences: Applications, Common Practice and Challenges, in: Schwartz, A.J., Kumar, M., Adams, B. L., Field, D.P. (Ed.), Electron Backscatter diffraction in Materials Science. Springer Science + Business Media, pp. 345-360. 10.1007/978-0-387-88136-2_26

Prior, D.J., Wheeler, J., Peruzzo, L., Spiess, R., Storey, C., 2002. Some garnet microstructures: an illustration of the potential of orientation maps and misorientation analysis in microstructural studies. Journal of Structural Geology 24, 999-1011. 10.1016/S0191-8141(01)00087-6

Randle, V., 1995. Microtexture Determination and it's Application. Institute of Materials, London.

Reddy, S., Timms, N.E., Pantleon, W., Trimby, P., 2007. Quantitative charaterization of plastic deformation of zircon and geological implications. Contrib mineral Petrol 153, 625-645. 10.1007/s00410-006-0174-4

Saeid, T., Abdollah-zadeh, A., Shibayanagi, T., Ikeuchi, K., Assadi, H., 2010. On the formation of grain structure during friction stir welding of duplex stainless steel. Materials Science and Engineering: A 527, 6484-6488. 10.1016/j.msea.2010.07.011

Schmidt, N.H., Olesen, N.O., 1989. Computer-aided determination of crystal-lattice orientation from electron-channeling patterns in the SEM. Canadian Mineralogist 27, 15-22.

Schwarzer, R.A., Field, D.P., Adams, B.L., Kumar, M., Schwartz, A., 2009. Present State of Electron Backsctter Diffraction and Prospective Developments, in: Schwartz, A.J., Kumar, M., Adams, B. L., Field, D.P. (Ed.), Electron Backscatter Diffraction in Materials Science. Springer Science + Business Media, pp. 1-20. 10.1007/978-0-387-88136-2_1

Siqueira, R.P., Sandim, H.R.Z., Oliveira, T.R., Raabe, D., 2011. Composition and orientation effects on the final recrystallization texture of coarse-grained Nb-containing AISI 430 ferritic stainless steels. Materials Science and Engineering: A 528, 3513-3519. 10.1016/j.msea.2011.01.007

Skemer, P., Katayama, I., Jiang, Z., Karato, S.-i., 2005. The misorientation index: Development of a new method for calculating the strength of lattice-preferred orientation. Tectonophysics 411, 157-167. 10.1016/j.tecto.2005.08.023

Thorvaldsen, A., 1997. The intercept method--2. Determination of spatial grain size. Acta Materialia 45, 595-600. 10.1016/S1359-6454(96)00198-X

Toy, V.G., Prior, D.J., Norris, R.J., 2008. Quartz fabrics in the Alpine Fault mylonites: Influence of pre-existing preferred orientations on fabric development during progressive uplift. Journal of Structural Geology 30, 602-621. 10.1016/j.jsg.2008.01.001

Trimby, P.W., Prior, D.J., 1999. Microstructural imaging techniques: a comparison between light and scanning electron microscopy. Tectonophysics 303, 71-81. 10.1016/S0040-1951(98)00263-7

Venables, J.A., Harland, C.J., 1973. Electron Backscattering Patterns - New Technique for Obtaining Crystallographic Information in Scanning Electron-Microscope. Philosophical Magazine 27, 1193-1200. 10.1080/14786437308225827

Wenk, H.R., 1985. Preferred Orientation in Deformed Metals and Rocks: an Introduction to Modern texture Analysis. Academic Press, London.

Zucali, M., Chateigner, D., Dugnani, M., Lutterotti, L., Ouladdiaf, B., 2002. Quantitative texture analysis of glaucophanite deformed uner eclogite facies conditions (Sesia-Lanzo Zone, Western Alps): comparison between X-ray and neutron diffraction analysis, in: DeMeer, S., Drury, M.R., DeBresser, J.H.P., Pennock, G.M. (Eds.), Deformation Mechanisms, Rheology and Tectonics: Current status and future perspectives, pp. 239-253.